The arid climate of the Namib desert has also been an important factor both in beneficiating primary ores with secondary minerals released by weathering, and in the prevention of leaching by meteoric waters of the secondary mineralisation derived from the primary ores. The considerable age of this desert would have allowed ample time for secondary enrichment processes to occur as is evident in particular from the numerous economically interesting secondary superficial occurrences.

3 INITIAL INVESTIGATIONS

3.1 Magnetic and radiometric colour-composite maps

Maps of the five separate aeromagnetic and radiometric surveys covering the western portion of the Damara orogenic belt, released by the Geological Survey on Open File, were combined at a scale of 1:125 000. These composites were then coloured in, with due regard to the different sensitivities and datums used for each survey in order to make the coloured intervals match as closely as possible between the respective surveys. Colour intervals of 50 nT were used for the aeromagnetic composite and 100 cps for the total-count contours of the airborne radiometric composite.
No contour maps of the K, U and Th channels were available and all important spectrometric data were recorded as peak-to-background ratios on the major anomalies of the total-count map. The resulting two colour composites were reduced photographically and are presented at a scale of 1:1 000 000 as Figs 3 and 4.

3.2 Correlation between magnetic and radiometric responses

The airborne radiometric and magnetic data covering the area were compared, with the aim of establishing any possible magnetic characteristics associated with uranium mineralisation. Two significant features were evident (Corner, 1975; Corner and Henthorn, 1978):

i) certain negative (low with respect to the normal field intensity) magnetic anomalies are unusual in that they occur over structures which, if magnetised by induction in the Earth's present magnetic field, should give rise to positive anomalies at these latitudes. These anomalies often pervade areas of varying geological structure, indicating that a large degree of magnetic homogenisation has taken place. It was evident that every known major occurrence of uranium in the alaskitic granites fell within such a magnetically anomalous zone.

   Comparison of the magnetic data with the geology, in mapped areas, showed these anomalies to be confined stratigraphically to rocks (and granitic equivalents) of the Etusis and (chiefly) the Khan Formations of the Nosib Group and, to a lesser extent, to the Rössing Formation of the Swakop Group. It was also apparent that they are not associated with these formations everywhere and mostly occur over anticlinal and, in particular, dome-type structural deformation, probably as a result of the higher frequency of exposure of these stratigraphic levels in such structures.

Examples of the negative magnetic anomalies in relation to the geology are shown for the Rössing deposit and for the Ida- and Hollands-dome occurrences in Figs 5a and 5b respectively. This relationship may also be seen in computer modelled section, A - B (Fig 17).

Although it cannot be said that the granitic uranium occurrences themselves can be directly located using magnetic techniques, their immediate geological environment is undoubtedly hallmarked by the negative magnetic anomalies. The anomalies, which are semi-regional in extent, thus delineate target areas in which granitic uranium occurrences might occur and thus form an important prospecting criterion.

Corner (1975) considered that the anomalies might arise from remagnetisation of the rocks, during the last phases of metamorphism and anatexis, in a magnetic field having a direction considerably different from that of the Earth's present-day field. Palaeomagnetic studies were therefore undertaken, utilizing the facilities of the Geological Survey of South Africa, in order to test this hypothesis. These are described in Section 4.

ii) A regional magnetic/radiometric correlation exists, in that areas characterised by positive (high with respect to the normal field intensity) magnetic anomalies often show high total-count gamma-ray responses. This correlation, which was first noted by Toens (1974 unpublished), occurs chiefly over the red granites and may be seen from Figs 3 and 4 and the interpretative overlay. Investigations on the ground showed that the anomalous radiometric responses result from the relative increase in thorium concentration within these rocks, often associated

Fig 5a Geology of the area in the environs of the Rössing dome, showing aeromagnetic contours (Legend contained in Fig 6)

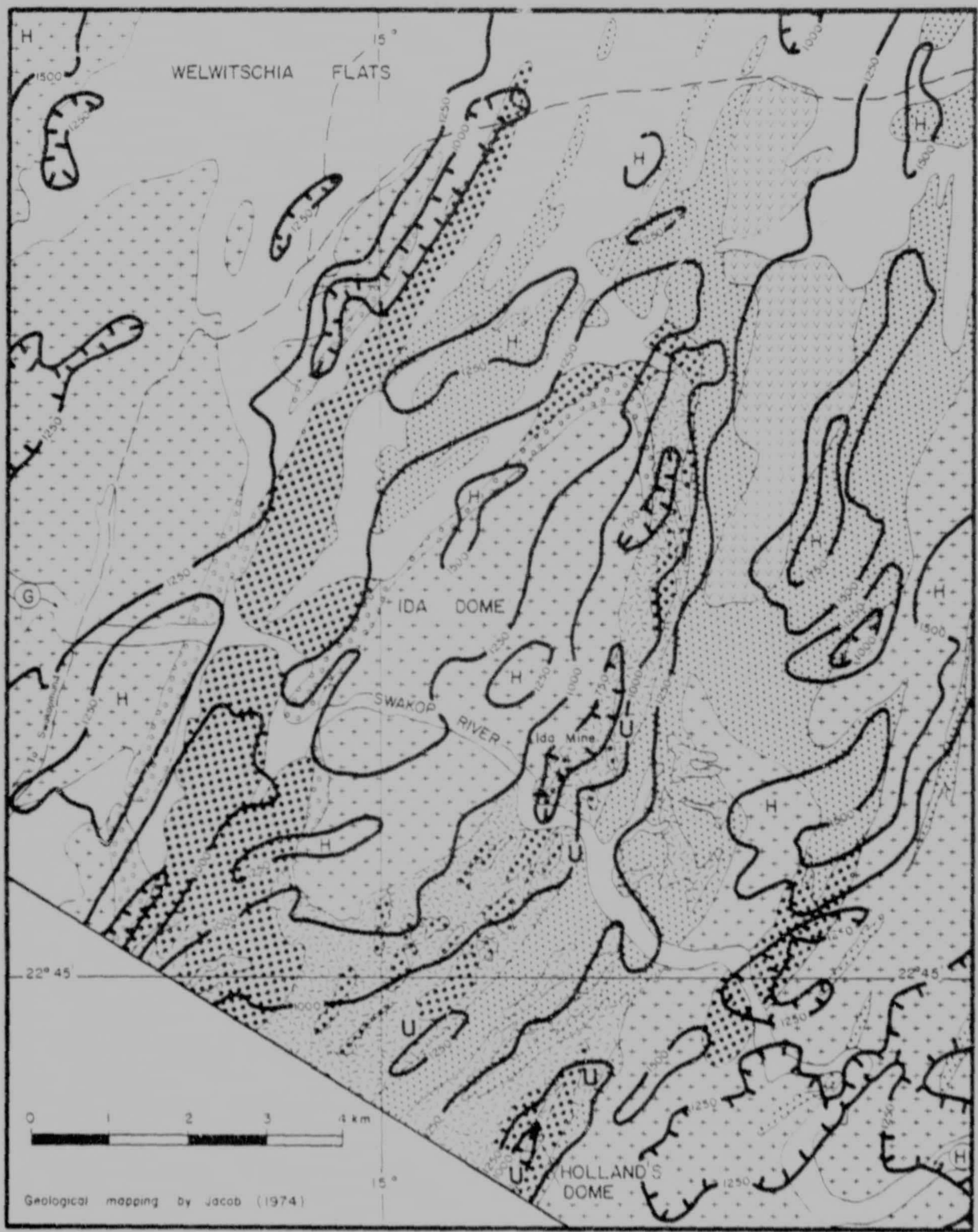

Fig 5b Geology of the area in the environs of the Ida dome, showing aeromagnetic contours (Legend contained in Fig 6)

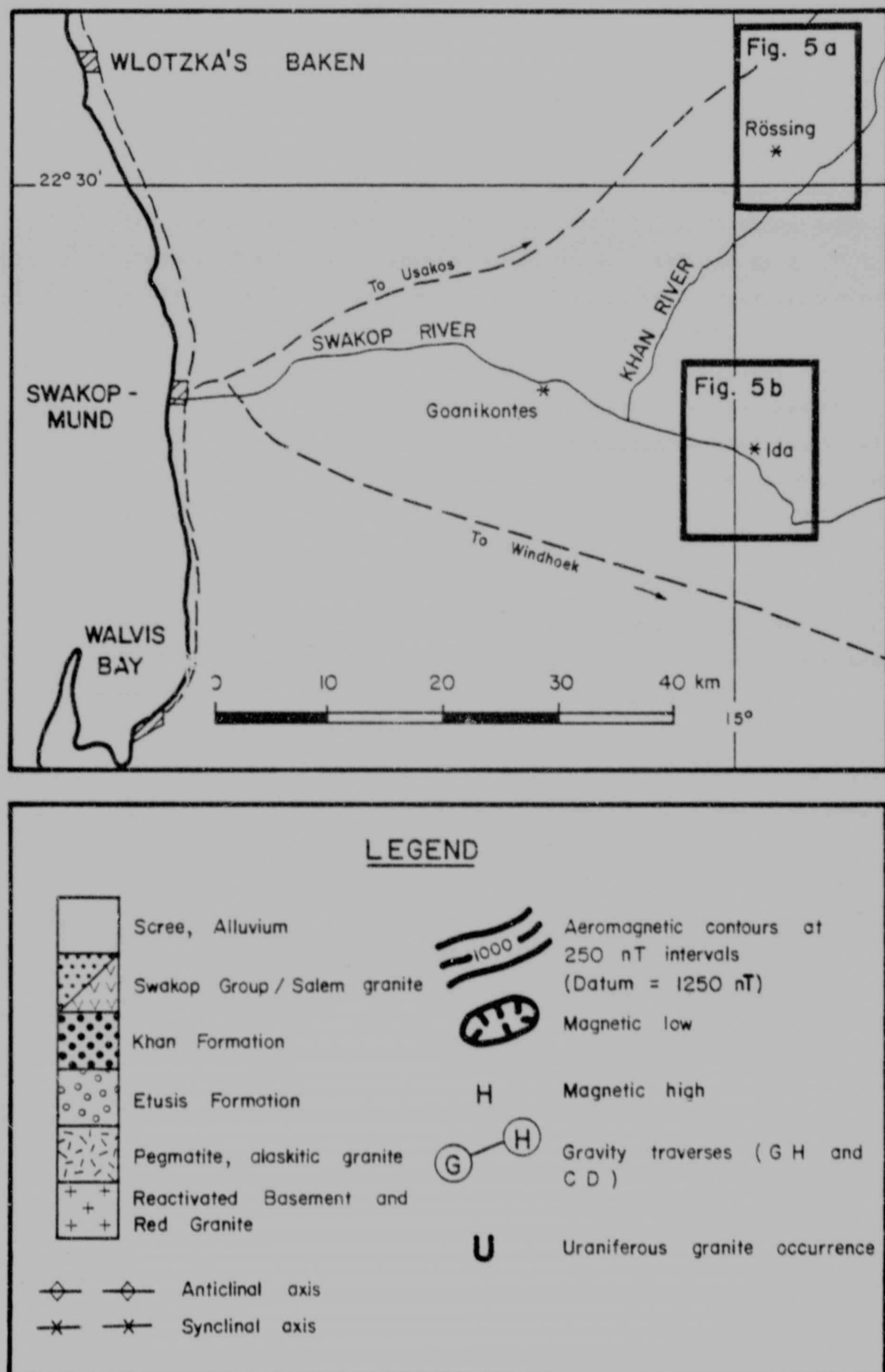

Fig 6 Locality map and legend for Figs 5a and 5b

with non-economic increases in the concentration of uranium. Although the overall concentrations of uranium and thorium are higher than in the surrounding rocks (up to 300 ppm U_3O_8 and 1 000 ppm ThO_2 have been recorded spectrometrically by the author), the increases are not necessarily uniform and some outcrops yield a radiation level raised only slightly above background. The higher magnetic responses over the red granites were initially thought to be due to relatively high concentrations of iron-rich minerals, especially magnetite. The palaeomagnetic results presented in Section 4 indicate, however, that these responses are due to a direction of magnetisation differing from both that of the 500 Ma tectonothermal event and from that of the Earth's present-day direction (i.e. a probable hybrid direction).

It is felt that the magnetic highs related to the red granites cannot be used directly as pathfinders to economic quantities of uranium, but are useful in mapping the subsurface geology in areas covered by surficial deposits.

Although numerous ground magnetic traverses were conducted in this study they were used primarily for location of anomalous zones rather than for interpretation. The reason for this is that the ground profiles are extremely noisy due to high concentrations of magnetic minerals, particularly in the Nosib Group. No ground profiles have therefore been included in this thesis and the aeromagnetic data have exclusively been used in preference for interpretation.

4 PALAEOMAGNETIC WORK

In view of the economic implications of the negative magnetic anomalies as outlined in Section 3, it was decided to investigate the cause of the anomalies and hence their use as a prospecting criterion in the search for uranium. Paleomagnetic measurements were made at the palaeomagnetic laboratory of the Geological Survey of South Africa. The success of the investigations was dependant on the assumption that the uraniferous alaskitic granites represent the last phase of tectonism, during which temperatures exceeded (up to 750°C, see Section 2.5) the Curie points of the magnetic mineral constituents and that, on cooling, little or no further movement or folding or substantial reheating of the rocks had occurred (Jacob 1974a).

Palaeomagnetic field work was conducted on two separate occasions - initially during May/June 1976 when 31 sites were sampled and subsequently during March/April 1978, bringing the total number of sampled sites to 48. The latter survey was conducted in order to resolve some of the points of ambiguity arising from the initial survey and also to establish a more complete palaeomagnetic record of the area. This was also considered to be necessary to facilitate the magnetic computer-modelling discussed in Section 5.2. The results of the initial survey have been reported previously (Corner and Henthorn, 1978) and are fully combined here with all subsequent data.

4.1 Field Procedure

Oriented core samples were taken, by means of a portable drill, from 46 sites in the area between the Brandberg-Messum-Cape Cross line in the North and the Kuiseb River in the South. An additional two sites were drilled into basement to the South of the Kuiseb River. The site locations are indicated on the generalised geological map of the area (Fig. 2). Four or five cores, each up to 10 cm in length, were drilled at each site and oriented by means of a sun compass. Orientations were also read using a magnetic compass as a check on the final core orientation. The cores, which were 2,5 cm in diameter, were subsequently cut up into 2,5 cm lengths, giving a total of 450 core specimens or an average of 9 specimens per site.

Thirty five sites were taken from rocks of the Damara Sequence of which 23 were obtained from the negative magnetic zones, mostly in close association with the uraniferous alaskitic granites, and 12 were obtained from areas of either normal or positive magnetic-field intensity. Of the 35 sites only 4 were collected from rocks of the Swakop Group and granitic equivalents in view of the relatively undisturbed magnetic field over these rocks. Seven sites were derived from the basement (granite-gneiss, Piksteel Granodiorite and rocks of the Abbabis Metamorphic Complex) and two each from the Cape Cross, Brandberg and Erongo intrusives. Only 24 localities are shown in Fig. 2 due to the close proximity of some of the localities and the small scale of the map. Table A1 in the Appendix gives the exact localities of the sites, the lithological units from which they were derived and the local intensity of the geomagnetic field (determined from the average of five readings at each site in order to reduce local variations).

4.2 Laboratory Instrumentation, Procedure and Results

4.2.1 Remanent magnetisation

Measurement of remanent magnetisation, both natural (NRM) and after alternating-field (AF) demagnetisation, was carried out using a Digico 'Complete Results' spinner magnetometer described by Molyneux (1971). A schematic diagram of the system is given in Fig 7a. The specimen may be placed, in any of six orientations, onto a cubic platform mounted on top of a vertical shaft (Fig 7a, 7b). The shaft is driven at 7 Hz by an induction motor. The phase relative to a reference signal produced by a slotted (128 slots) 'chopper' disc at the bottom of the shaft, determines two orthogonal components of magnetisation in a plane perpendicular to the axis of rotation as shown below:

SPIN ORIENTATION (Fig 7b)	ORTHOGONAL COMPONENTS: A	B
1	+Z+a	-Y+b
2	+Z+a	-X+b
3	-Z+a	+Y+b
4	-Z+a	+X+b
5	+X+a	+Y+b
6	+X+a	-Y+b

'a' and 'b' are the orthogonal components of the platform in a plane perpendicular to the axis of rotation, and X, Y and Z are the orthogonal components defining the direction of magnetisation. The magnetisations in columns A and B are summed after the fourth spin orientation and divided by four to give values for 'a' and 'b'. The X and Y components are overdetermined by the fifth and sixth spins thus placing greater confidence in the accuracy of their derived amplitudes. When the desired number of spins has been completed the stored wave-forms, measured by the fluxgate sensors, are subjected to Fourier Analysis to yield the fundamental two orthogonal components for a particular orientation as indicated above. The final output is the amplitude and direction (Fig 7b) of the vector of magnetisation. The measurement time increases linearly with the number of spins whereas random noise decreases with the square root of the measurement time.

Alternating-field demagnetisation was carried out on an apparatus based on that described by McElhinny (1964). The specimen was tumbled, by rotation about two orthogonal axes and prec[illegible] about a third, in the centre of a coil through which a decaying [illegible] current flowed. This randomised all magnetic domains having coercivities below the maximum field produced by the peak (initial) current. The maximum field that could be achieved by the coil was 100 mT which is significantly less than that (200 mT) obtainable from the apparatus described by McElhinny. Since most coercivities of secondary magnetisation are less than ± 80 mT and since the Damara virtual geomagnetic pole position derived in this study is consistent with data of other researchers (section 4.3.6), it is felt that this limitation has in no way affected the conclusions arrived at. The whole apparatus was contained in Helmholtz coils to annul the Earth's magnetic field. The tumbling of the specimen in the above manner was designed to present all axes to the coil while randomising any anhysteretic remanent magnetisation. Secondary, unstable components of magnetisation were thus reduced to levels small compared with the primary component (Wilson and Lomax, 1972; Hailwood and Molyneux, 1974; Edwards, 1980).

The NRM of each core specimen was measured and one or two specimens per site were set aside for subsequent thermal demagnetisation studies. At least one specimen per site was initially demagnetised in an alternating field, in steps of 5, 10 or 20 mT up to 100 mT. If the direction of magnetisation remained stable i.e. showed no significant change with respect to the NRM direction, the remaining core specimens were demagnetised in a single step, in an alternating field of 80 mT. For those sites which

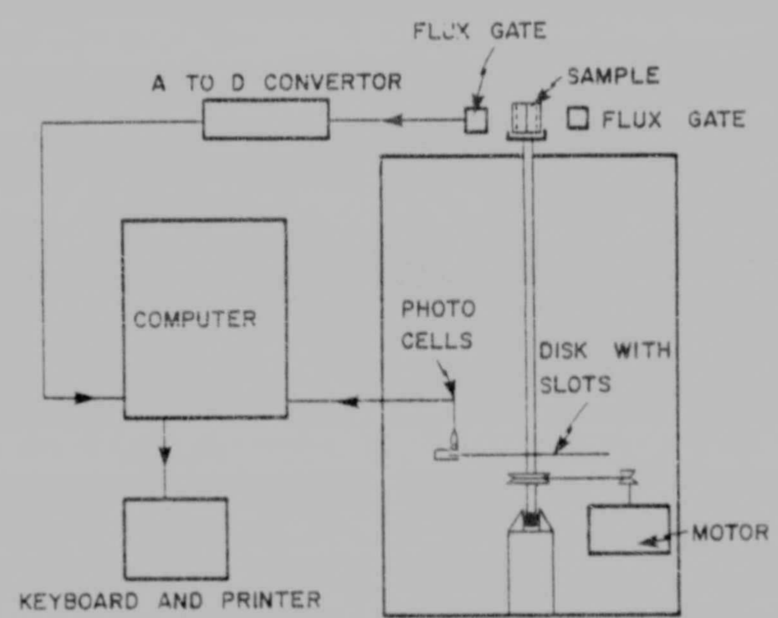

Fig 7a Schematic diagram of the spinner magnetometer system (after Molyneux, 1971)

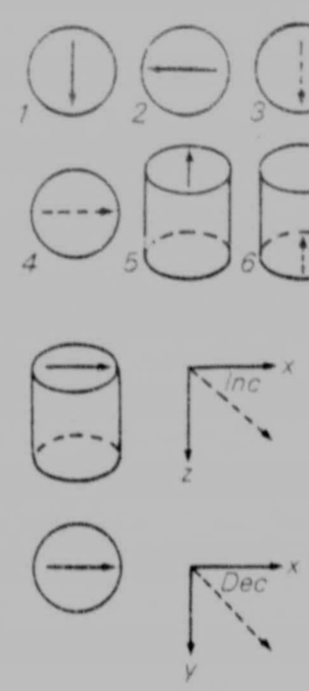

Fig 7b Spin orientations with respect to the fiducial mark. The magnetisation vector is defined by the indicated declination and inclination and its intensity given by $(X^2+Y^2+Z^2)^{\frac{1}{2}}$.

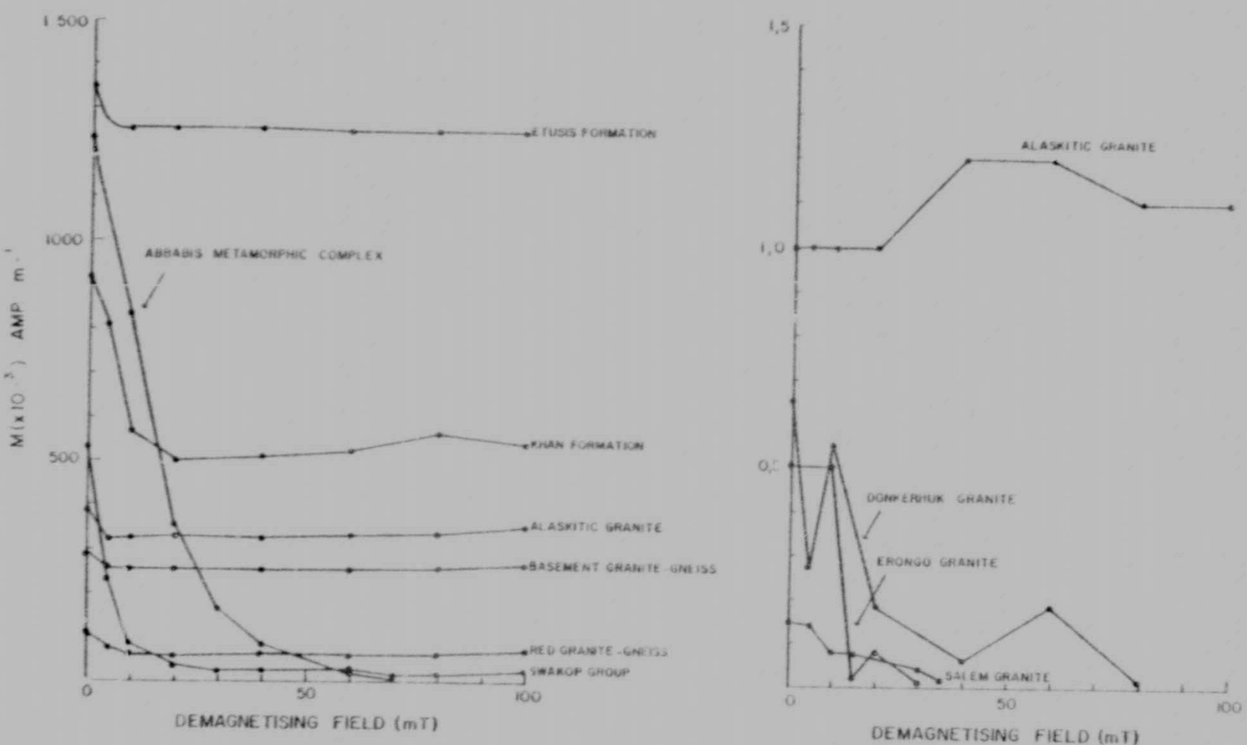

Fig 8 Som.. typical alternating-field demagnetisation responses.

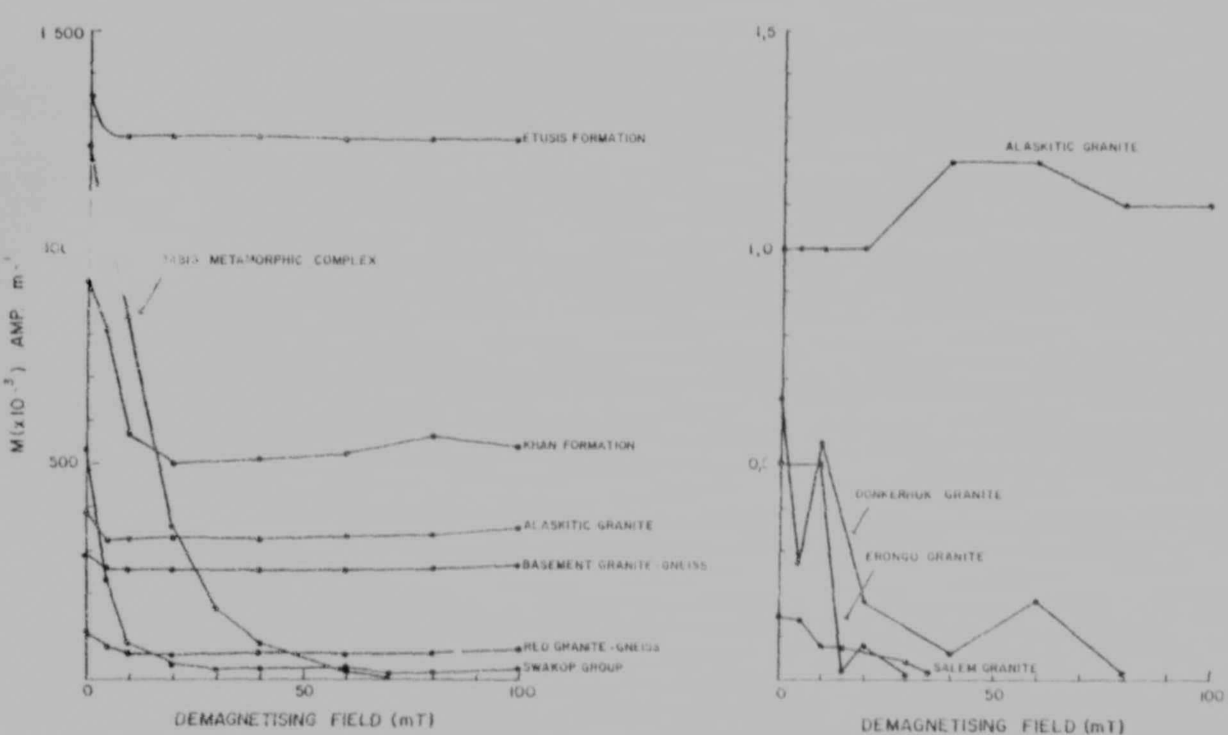

Fig 8 Some typical alternating-field demagnetisation responses.

yielded scattered NRM directions and/or directional instability, the remainder of the cores were also subjected to step-by-step demagnetisation up to the limit of the AF apparatus (i.e. 100 mT) or until the intensity of magnetisation fell to a level below the accuracy of the instrument ($0,1 \times 10^{-3}$ $A.m^{-1}$ or 1% of the undemagnetised NRM intensity). The NRM and AF-demagnetised directions were plotted stereographically for each site and are given in the Appendix. The site-mean directions are presented in Table II, together with the relevant Fisher statistics (Fisher, 1953, Section 4.2.2 below), for all those sites which yielded a significant grouping in terms of the randomness parameter R (Irving, 1964). The ranges of intensity of magnetisation, measured for the core specimens, are given in Table III. A large degree of lithological heterogeneity is evident from the measured ranges, particularly for the Nosib Group, basement and granitic equivalents. No structural corrections were applied to any of the sites, in view of the overall good grouping of site-mean directions (Fig 12) as discussed in Section 4.3.1. Some typical Af-demagnetisation responses are shown in Fig 8.

It should be noted that at the time of commencement of this study the 'blanket' demagnetisation techniques employed were recommended by the Geological Survey. The value of orthogonal vector plotting techniques as a guide to isolating vector directions (Zijderveld, 1967; Stupavsky and Symons, 1978; and Dunlop, 1979) was only brought to the attention of the author at a late stage. Fortunately, however, this limitation is more apparent than real since many of the Nosib sites yielded directions after AF demagnetisation statistically unchanged from the NRM directions. The secondary magnetisation which affected certain sites and which yielded scattered within-site NRM directions (sites 10, 12, 15, 17, 18, 27, 28, 41) was of low coercivity and readily removed by AF demagnetisation at low fields (less than ± 50 mT). Apart from this 'soft' magnetisation, essentially only one component of magnetisation consistently resulted for the Nosib rocks and related granites within the available demagnetising range of the apparatus. In retrospect, therefore, it is felt that Zijderveld-type techniques would not have yielded any additional information of major significance to this study for these lithological units. Nevertheless these techniques may be of great value for the other sequences which do not display strong remanence e.g. Swakop Group, basement rocks (granite-gneiss and Abbabis Complex) and the late intrusives. This should be borne in mind for future research.

4.2.2 Statistical treatment of the data

The statistical parameters provided by the Digico software package and quoted throughout this thesis are those derived by Fisher (1953) for the estimation of precision of measurements-of-position on a sphere.

Fisher assumes the fundamental distribution of elementary errors over the surface of a sphere to have a frequency density proportional to

$$e^{k \cos \Theta}$$

where Θ is the angular displacement of a measurement from the true position, i.e. for $\Theta = 0$ the density is a maximum for positive k.

k is a measurement of precision and, for large k, the distribution is effectively confined to a small portion of the sphere in the neighbourhood of the maximum. For k tending to 0 the distribution approaches uniformity of scatter over the spherical surface.

Now, given a sample of points dispersed from a common centre, the estimate of the position of this centre is found by making S(CosΘ) a maximum, where S signifies summation over the sample set. The estimated direction is that of the vector sum of unit vectors having the directions of several observations. This vector sum is given by the parameter R (termed the randomness parameter by Irving (1964) defined by

$$R^2 = S^2(\ell) + S^2(m) + S^2(n)$$

where ℓ, m and n are the direction cosines of any observed point. Thus, as R approaches its maximum, n, the number of observations (in this case, the number of core-specimen directions) the more significant is the grouping.

$\alpha 95^{\circ}$ as used in this text is the semi-vertical angle of a cone about the mean direction at the 95% level of confidence. It is obvious that the smaller the value of $\alpha 95^{\circ}$ the closer is the distribution of sample points to the true mean value.

The relative magnitude of R (with respect to n), k and α_{95}^{o} were carefully assessed in deciding upon the statistical validity of the derived directions (Table II).

4.2.3 Magnetic susceptibilities and Koenigsberger ratios

The Digico system allowed for measurement of susceptibility by introduction of the core specimen into a coil system. The impedance and hence the output from a secondary winding of the coil system was thereby varied and calibrated using a standard specimen provided with the instrument. In this manner the susceptibility of each core-specimen was measured and the range and mean of the values derived for each site are presented in Table IV.

In view of its value as guide in assessing the dominance of remanent magnetisation as opposed to induced magnetisation, the Koenigsberger ratio was calculated for each core specimen using the relation.

$$\text{Koenigsberger ratio (Q)} = \frac{M}{kF}$$

where M is the intensity of natural remanent magnetisation
k is the magnetic susceptibility
F is the intensity of the local magnetic field.

The range and mean of the values thus determined are also listed in Table IV. The susceptibilities and Koenigsberger ratios given in Table IV are also presented graphically in Fig 9.

4.2.4 Thermal demagnetisation

A slightly modified form of the apparatus described in Section 4.2.1 enabled continuous thermal demagnetisation to be carried out (Creer, 1967; Molyneux, 1971). The system uses the same computer apparatus but the rotating mechanism is inverted so that the specimen hangs into a furnace which is insulated by a double dewar system and water-cooled shielding. The flux gate system remains outside at room temperature and it was thus possible to measure the remanence at the elevated temperature, obviating the need for cooling in a field-free space. The greater distance between the flux gate system and the specimen decreased the signal strength and it was therefore necessary to use longer measurement times. The rotating mechanism allowed measurement only at two orientations of the specimen.

TABLE II : APPROXIMATE SITE LOCALITIES AND SITE-MEAN DIRECTIONS (AFTER A.F. DEMAGNETISATION)

SITE NUMBER	APPROXIMATE LOCALITY	LITHOLOGICAL UNIT	SITE - MEAN		FISHER STATISTICS*			
			DECLINATION°	INCLINATION°	k	α95°	R	n
01	Rössing Mine	Alaskitic granite	334,2	61,1	28	9,9	8,71	9
02	Rössing Mine	Khan Formation	344,6	59,4	164	3,5	10,94	11
03	Rössing Mountain	Khan Formation	322,7	44,4	9,0	19,4	7,23	8
04	Rössing Dome	Red granite	329,7	54,5	23	11,8	7,69	8
06	Valencia	Alaskitic granite	350,5	-58,4	9,1	21,0	6,35	7
07	Valencia	Etusis Formation	325,5	44,7	180	3,2	11,93	12
08	Valencia	Etusis Formation	299,0	54,0	7,6	35,4	3,61	4
09	Valencia	Etusis Formation	316,9	29,4	15	11,2	12,18	13
10	Palmenhorst	Khan Formation	331,7	68,7	181	4,1	7,96	8
11	Palmenhorst	Alaskitic granite	336,8	44,1	11	17,4	7,36	8
12	Palmenhorst	Red granite	18,2	62,4	30	12,4	5,83	6
**13A	Trekkopje	Etusis Formation	322,1	68,1	90	13,0	2,98	3
13B	Trekkopje	Etusis Formation	23,5	-53,4	44	9,1	6,86	7
15	Trekkopje	Red granite	339,6	66,9	72	5,7	9,87	10
17	Tsaun Beacon	Alaskitic granite	319,7	58,9	4,6	31,5	5,70	7
18	Tsaun Beacon	Khan Formation	344,5	50,2	52	6,4	10,81	11
19	Tsaun Beacon	Khan Formation	145,2	-19,3	245	3,8	6,97	7*
20	Kuiseb river	Basement granite-gneiss	156,1	-30,4	136	4,4	8,94	9
21	Kuiseb river	Basement granite-gneiss	151,4	-34,2	166	3,5	10,94	11
22	Hollands Dome	Alaskitic granite	348,3	48,3	101	4,8	9,91	10
**23A	Hollands Dome	Khan Formation	316,7	32,9	322	6,8	2,99	3
23B	Hollands Dome	Khan Formation	2,6	-43,2	27	10,3	7,74	8
24	Hollands Dome	Alaskitic granite	323,4	58,9	11	17,1	7,39	8
25	Ida Mine	Khan Formation	338,2	62,2	44	6,9	10,77	11
26	Ida Mine	Alaskitic granite	340,5	50,2	8,0	18,1	8,87	10
27	Ida Mine	Alaskitic granite	345,2	57,5	21	10,1	10,53	11
28	Hollands Dome	Red granite	351,0	62,3	56	10,3	4,93	5
**29A	Ida Dome	Alaskitic granite (Inside halo)	352,6	49,2	10	17,4	8,17	9
29B	Ida Dome	Alaskitic granite (Outside halo)	344,3	-50,6	26	18,4	3,88	4
32	Solitaire	Piksteel Granodiorite	105,1	-53,9	139	6,5	4,97	5
33	Saagberg	Piksteel Granodiorite	148,1	-47,6	149	5,5	5,97	6
34	Abbabis	Basement granite-gneiss	8,7	33,4	288	3,9	5,98	6
35	Ubib	Abbabis Met. Complex	104,7	48,9	7,6	25,9	5,34	6
37	Cape Cross	Basalt	299,8	-44,8	29	9,1	9,69	10
38	Cape Cross	Basalt	298,0	-34,5	1 295	1,5	7,99	8
39	Tsaun Beacon	Khan Formation	345,1	50,0	245	3,2	8,97	9
40	Tsaun Beacon	Khan Formation	342,2	46,5	408	2,5	8,98	9
41	Tsaun Beacon	Khan Formation	61,5	66,5	2,5	47,4	4,67	7
43	Brandberg	Brandberg granite	0,2	-31,8	65	7,5	6,91	7
44	Anibib	Erongo granite	330,2	-57,0	51	9,4	5,90	6
45	Ameil	Erongo granite	324,7	-38,2	18	22,3	3,83	4
46	Wlotska's Baken	Khan Formation	171,3	-22,4	30	11,1	6,80	7
47	Goanikontes	Swakop Group	72,6	-54,5	4,1	33,9	5,54	7

* Fisher statistics after A.F. demagnetisation (see Appendix A2 for stereographic plots and demagnetising field values)
k is Fisher's precision parameter
α95° is the semi-vertical angle of the cone of 95% confidence about the mean direction
R is the randomness parameter, i.e. as R approaches n, the more significant the grouping
n is the number of oriented core specimens
** Sites yielding two significantly different directions

TABLE III : RANGES OF INTENSITIES OF MAGNETISATION (M)

FORMATIONAL UNIT		SITE NUMBER	RANGE OF M ($X10^{-3}$ $A.M^{-1}$)	
			SITE RANGE	TOTAL RANGE
BRANDBERG GRANITE		42	70 - 150	70 - 240
		43	160 - 240	
CAPE CROSS INTRUSIVES		37	516 - 830	516 - 1 563
		38	1 275 - 1 563	
ERONGO GRANITE		44	10 - 48	0,2 - 48
		45	0,2 - 0,5	
DONKERHUK GRANITE		30	0,27 - 0,75	0,17 - 0,75
		31	0,17 - 0,60	
SALEM GRANITE		16	0,1 - 2,5	0,1 - 2,5
SWAKOP GROUP		47	0,5 - 1,1	0,5 - 1,1
ALASKITIC GRANITE (LEUCOGRANITE)		01	20 - 890	0,1 - 5 250
		06	0,1 - 0,65	
		11	0,84 - 2,85	
		14	42 - 5 250	
		17	0,2 - 1,0	
		22	290 - 410	
		24	4 - 52	
		26	24 - 1 090	
		27	20 - 72	
		29	7 - 895	
RED GRANITE		04	560 - 7 570	0,3 - 7 570
		05	17 - 236	
		12	30 - 386	
		15	1 790 - 4 640	
		28	0,9 - 2,1	
		48	0,3 - 2,3	
KHAN FORMATION		02	21 - 536	21 - 8 050
		03	1 950 - 8 050	
		10	122 - 330	
		18	210 - 1 050	
		19	360 - 920	
		23	210 - 1 130	
		25	870 - 1 375	
		39	260 - 475	
		40	1 115 - 1 545	
		41	60 - 145	
		13	2 540 - 7 630	
		46	180 - 1 210	
ETUSIS FORMATION		07	260 - 710	50 - 1 340
		08	260 - 1 340	
		09	50 - 1 060	
BASEMENT	GRANODIORITE	32	15 - 36	1,8 - 2 045
		33	1,8 - 8,6	
	GRANITE-GNEISS	20	168 - 620	
		21	103 - 345	
		34	10 - 30	
	ABBABIS MET. COMPLEX	35	940 - 2 045	
		36	10 - 320	

TABLE IV : SUSCEPTIBILITIES AND KOENIGSBERGER RATIOS OF SITES INVESTIGATED

FORMATIONAL UNIT	SITE NUMBER	SUSCEPTIBILITY ($X10^{-6}$, SI)		KOENIGSBERGER RATIO		REMARKS*
		RANGE	MEAN	RANGE	MEAN	
BRANDBERG GRANITE	42	2 240 - 3 460	2 580	1,0 - 2,7	1,7	Unstable
	43	4 810 - 7 060	5 660	1,1 - 1,6	1,4	Unstable
CAPE CROSS INTRUSIVES	37	2 430 - 3 860	[illegible] 930	7,6 - 10,5	8,8	Stable
	38	25 800 - 29 700	27 660	1,9 - 2,7	2,2	Stable
ERONGO GRANITE	44	46 - 380	210	1,1 - 41	13	Stable
	45	50 - 65	55	0,2 - 0,3	0,3	Unstable
DONKERHUK GRANITE	30	45 - 72	50	0,2 - 0,6	0,4	Unstable
	31	63 - 84	74	0,1 - 0,3	0,2	Unstable
SALEM GRANITE	16	2 - 60	50	0,1 - 2,0	0,4	Unstable
SWAKOP GROUP	47	93 - 150	115	0,2 - 0,5	0,3	Unstable
ALASKITIC GRANITE	01	1,3 - 21	7,5	63 - 1 603	648	Stable
	06	5,0 - 38	15	0,1 - 4,4	1,8	Unstable
	11	24 - 45	29	0,8 - 4,9	2,7	Stable
	14	176 - 6 120	2 790	3,6 - 41	16	Unstable
	17	0,3 - 14	2,5	1,0 - 93	34	Unstable
	22	0,5 - 15	10,0	1 029 - 1 741	1 439	Stable
	24	14 - 50	29	5,9 - 68	31	Stable
	26	2,3 - 465	110	14 - 2 165	406	Stable
	27	1 460 - 8 660	3 380	0,2 - 0,9	0,5	Unstable
	29	2,0 - 87	50	25 - 619	132	Stable (TRM + CRM)
RED GRANITE	04	18 - 86	47	1 320 - 4 230	[illegible] 528	Stable
	05	75 - 27 000	4 750	0,7 - 10,5	2,8	Unstable
	12	1 820 - 13 600	8 170	0,2 - 2,1	0,9	Unstable
	15	18 130 - 42 980	30 420	2,7 - 6,7	4,4	Unstable
	28	9,8 - 14	11	2,9 - 8,2	4,8	Unstable
	48	6,3 - 18	11	1,4 - 10,6	3,7	Unstable
KHAN FORMATION	02	163 - 226	188	13 - 121	50	Stable
	03	640 - 905	820	104 - 421	193	Stable
	10	5 500 - 37 000	18 100	0,2 - 1,0	0,7	Unstable
	18	10 250 - 33 700	21 470	0,3 - 1,4	0,8	Unstable
	19	528 - 1 500	905	13 - 39	28	Stable
	23	5 260 - 23 800	9 260	1,3 - 9,6	3,4	Unstable
	25	125 - 265	188	203 - 272	250	Stable
	39	62 - 79	69	175 - 238	210	Stable
	40	65 - 97	78	523 - 784	689	Stable
	41	12 080 - 20 030	16 680	0,2 - 0,4	0,3	Unstable
	46	302 - 728	465	20 - 58	34	Stable
ETUSIS FORMATION	07	23 - 176	100	93 - 607	339	Stable
	08	19 - 84	49	131 - 970	550	Stable
	09	63 - 176	98	22 - 706	217	Stable
	13	578 - 1 240	754	126 - 370	257	Stable (TRM + CRM)
BASEMENT — GRANODIORITE	20	88 - 6 090	3 110	4 - 115	49	Stable
	21	176 - 13 650	2 700	1,0 - 36	7	Stable
BASEMENT — GRANITE-GNEISS	32	86 - 215	163	4,3 - 7,2	5,8	Partially Stable
	33	100 - 150	125	0,7 - 2,3	1,1	Stable
	34	20 - 36	30	21 - 36	26	Partially Stable
BASEMENT — ABBABIS MET. COMPLEX	35	31 400 - 49 000	42 200	1,1 - 1,7	1,4	Partially Stable
	36	1 460 - 36 000	9 760	0,2 - 0,4	0,3	Unstable

* Stability of remanence of either TRM (mostly) or CRM to AF demagnetisation

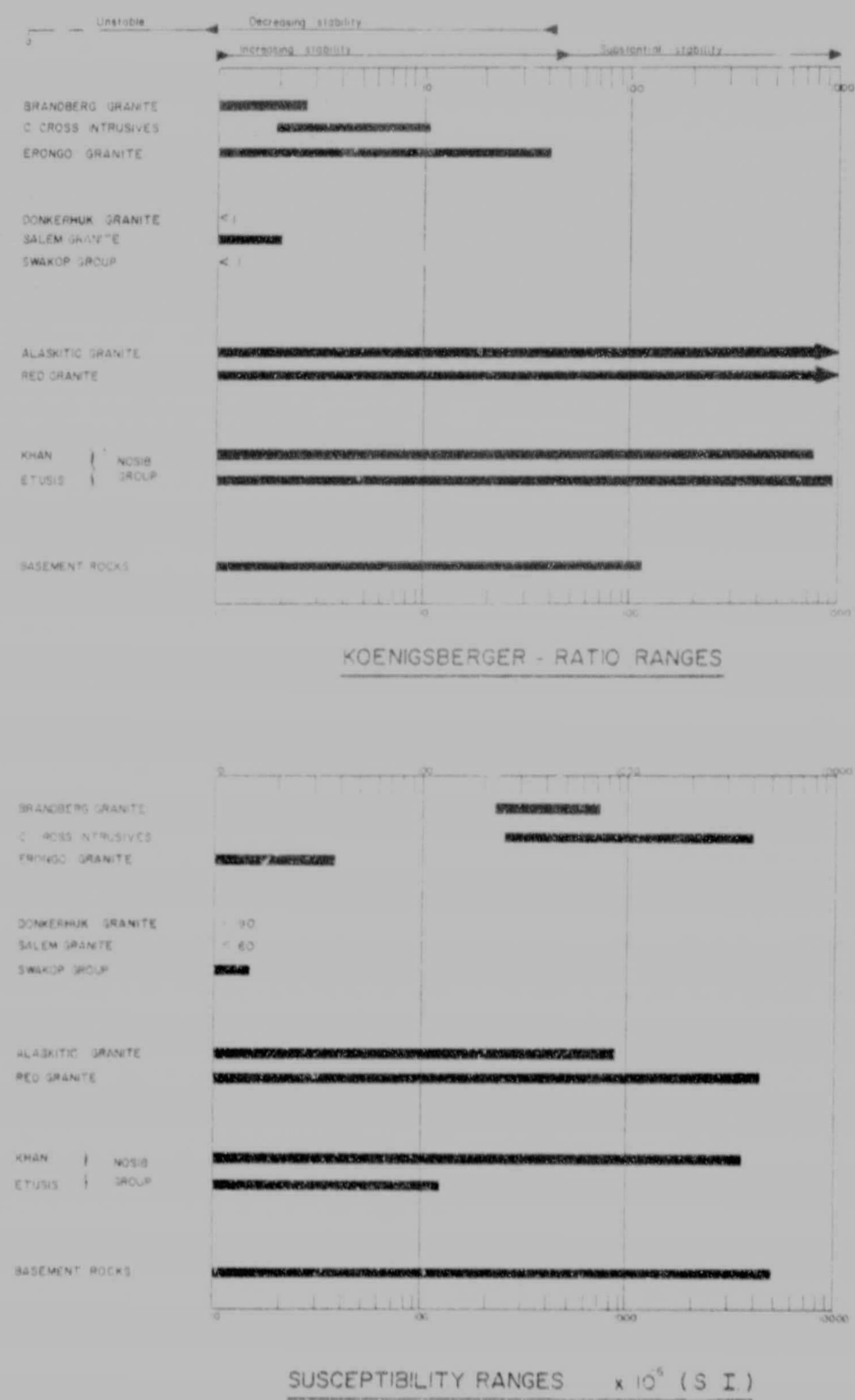

Fig 9 Ranges of Koenigsberger-ratios and susceptibilities (the relationship of stability of magnetisation to AF demagnetisation is qualitatively shown with respect to the Koenigsberger ratios at the top of the figure)

At least one core per site was retained for thermal demagnetisation studies. Only 19 cores from 17 different sites were, however, initially selected and demagnetised thermally. Thermal demagnetisation was carried out in steps of 100°C initially and, as the Curie point was approached, this was reduced to intervals of 50°C and 25°C. Since the directions of magnetisation either remained stable at the elevated temperatures or yielded new directions similar to those achieved by AF demagnetisation (excepting for sites 34 and 46, see Section 4.3.3) no further thermal demagnetisation work was conducted.

The variations in directions of magnetisation with increasing temperature are plotted stereographically in Fig 10 for the sites investigated and the corresponding thermomagnetic responses are given in Fig 11.

4.3 Discussion of the Results

4.3.1 Stability and mean directions of magnetisation after AF-demagnetisation

It was evident that certain lithologies displayed a marked stability in the direction of magnetisation during the course of progressive demagnetisation, i.e. no significant change occurred in the NRM direction. In comparing this stability, assumed to be indicative of the retention of remanent magnetisation, with the calculated Koenigsberger ratios, all sites with ratios above ± 35 were substantially stable whereas those with ratios below 1,0 were unstable. In the intermediate range (i.e. 1,0 - 35) certain sites retained their NRM directions whilst others were unstable, with a greater number of sites showing instability at lower ratios - typically below 5,0. Fig 9 shows this general relationship for the respective formational units. The instability in the directions of magnetisation to AF demagnetisation, indicative of a large component(s) of secondary magnetisation, may be seen from the stereographic plots in the Appendix.

The Nosib rocks and granitic equivalents, as well as the basement rocks, have thus largely retained their thermoremanent direction of magnetisation and display substantial stability of direction to AF demagnetisation. The same cannot, however, be readily said of the younger intrusives and particularly of the Swakop Group rocks in which the magnetisation is probably secondary (Section 4.3.1 - Swakop Group rocks and granitic equivalents). Further categorisation of stability in terms of the formational units is complicated by the dependance of remanence on grain size, mineralogical composition and possibly residual stress and grain shape (Day, 1977 ; Nagata, 1961),

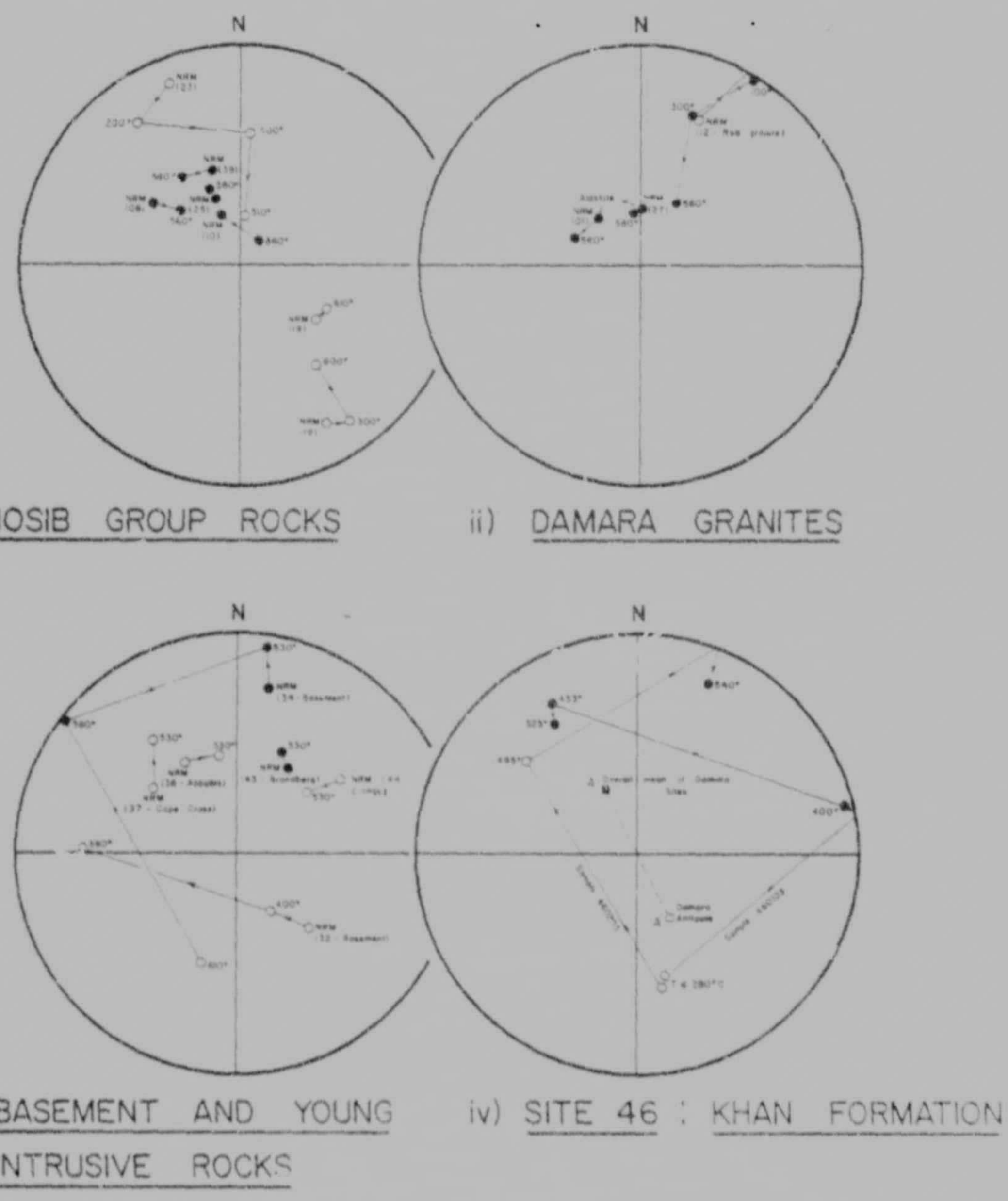

Fig 10 Variations in direction of magnetisation with increasing temperature

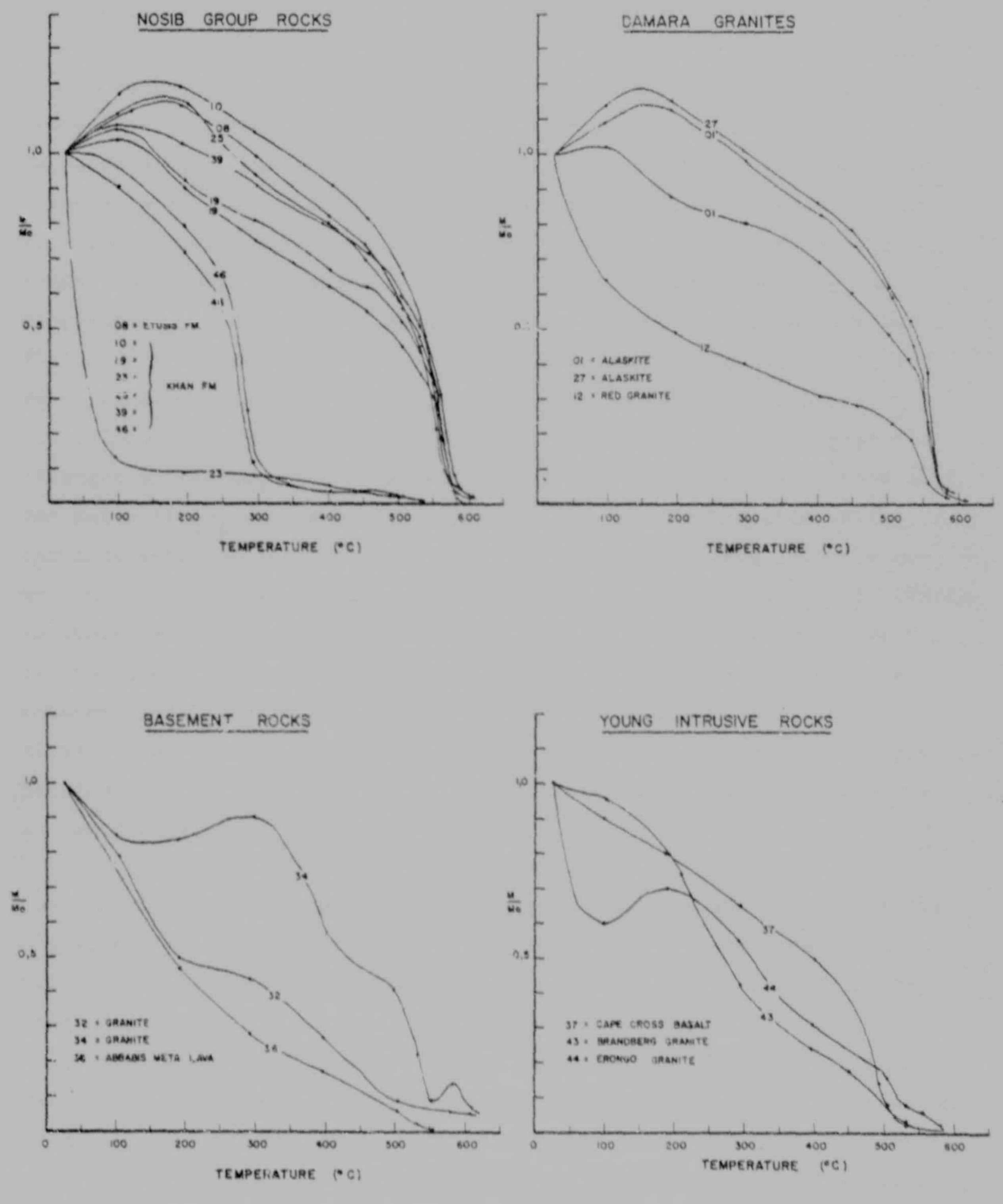

Fig 11 Thermal dema;netisation responses

and Stacey and Banerjee (1974) show that the stability of magnetisation in granular magnetic minerals generally increases with a decrease in grain size, resulting in a corresponding decrease in susceptibility. Groundmass magnetites may thus be expected to show a greater stability than phenocryst phases. Day (1977) has summarised the results of numerous workers with respect to the effects of particle size on magnetic properties of titanomagnetites. Coercivities and remanence are seen to increase with decreasing particle size following a power law (Coercive force $Hc \propto d^{-n}$, where d is the particle size and $0,4 < n < 0,9$). The coercive force attains a maximum at, or just below, the single domain transition size. The above pattern is, however, complicated by the contrasting properties of single-domain, and pseudo-single-domain particles, e.g. magnetite may be exsolved in feldspar phenocrysts, acting as a pseudo-single domain of high coercivity and strong remanence. Mineralogical composition may also significantly affect the magnetic hardness of the magnetic material. Stacey and Banerjee (1974) show that for $FeTiO_3/Fe_2O_3$ ratios of 0,2 - 0,4 in the ilmenite-hematite series, characteristic of certain of the Nosib sites sampled (Fig 13), the coercive force is high, resulting in a strong remanence. Day et al. (1976), in studying the magnetic properties of fine grained and single-domain titanomagnetites, showed an increase in magnetic hardness (and hence in remanence) with increasing titanium content. Multi-domain titanomagnetites did not, however, show any systematic variations in magnetic properties with composition, suggesting significant effects of inclusions on coercivity.

The majority of sites thus remained stable to AF demagnetisation or displayed a significant improvement in grouping after AF demagnetisation, with no statistically significant change in direction. This indicated that only single components of remanence existed for each formational unit, i.e. significantly wide windows in the coercivity spectra which were free of overlap were not prevalent in the available demagnetisation range of the instrumentation. It is possible that components of magnetisation, with coercivities higher than the demagnetisation capabilities, are present. The virtual geomagnetic pole result (4.3.6) for the Nosib rocks however, supports the fact that the single component measured does in fact clearly relate to the 450-550 Ma thermal event.

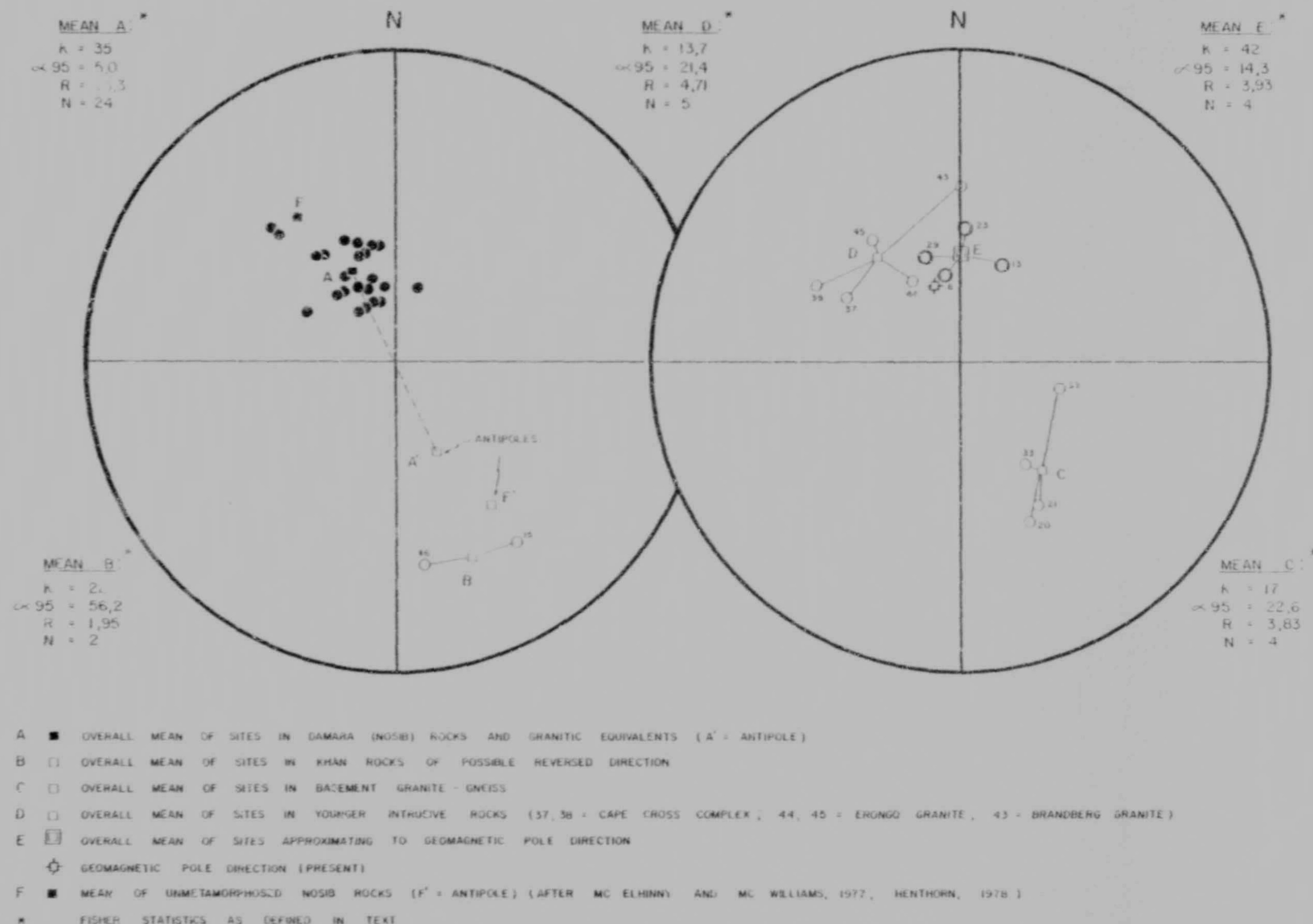

Fig 12 Wulff projection of site-mean magnetisation directions of Damara Sequence and basement rocks, and of late-, to post-Karoo intrusives (north seeking vector on upper hemisphere, open symbols; on lower hemisphere, closed symbols. The primitive plane is the present horizontal at the sampling sites).

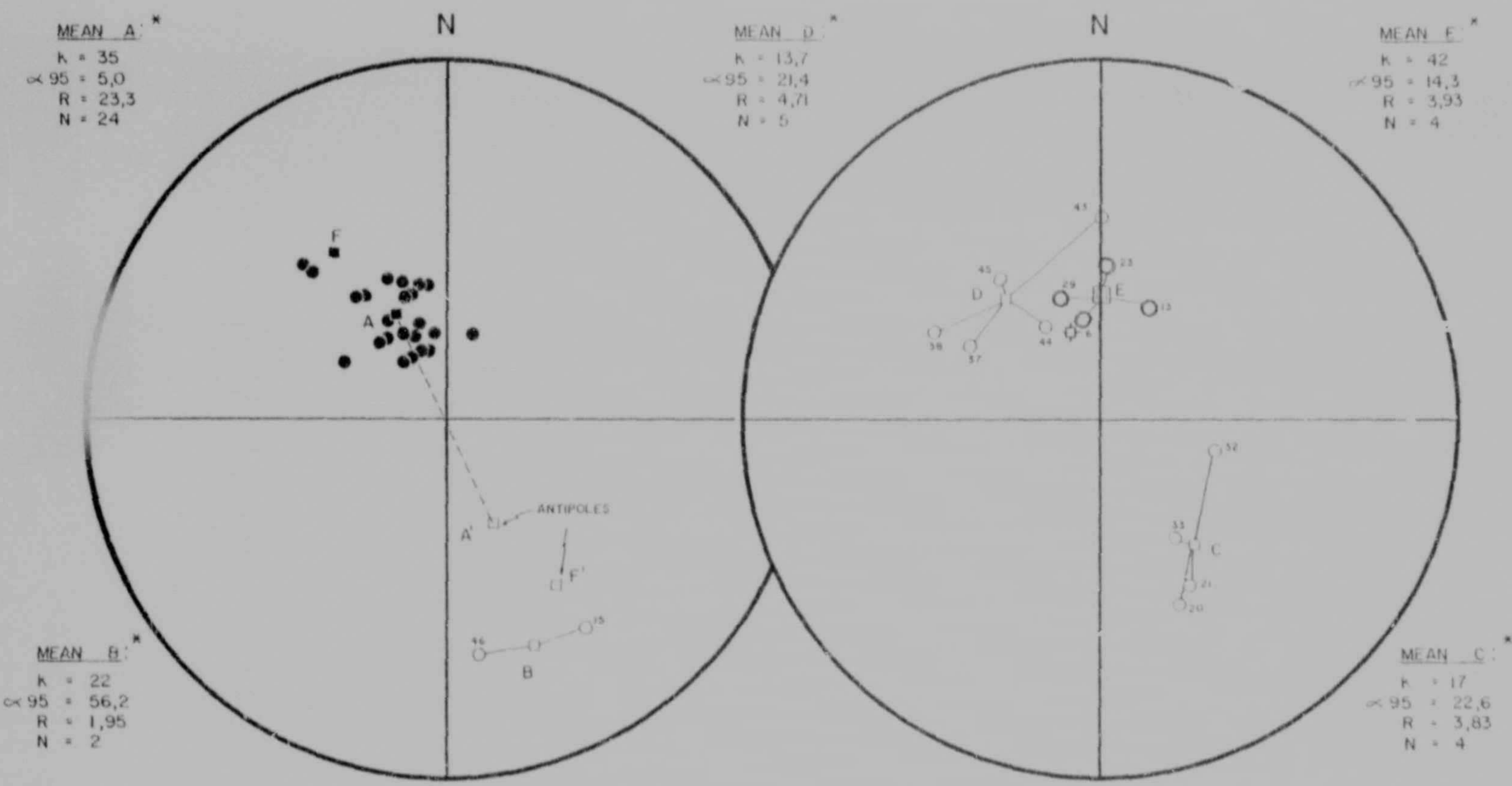

A ■ OVERALL MEAN OF SITES IN DAMARA (NOSIB) ROCKS AND GRANITIC EQUIVALENTS (A' = ANTIPOLE)

B □ OVERALL MEAN OF SITES IN KHAN ROCKS OF POSSIBLE REVERSED DIRECTION

C □ OVERALL MEAN OF SITES IN BASEMENT GRANITE - GNEISS

D □ OVERALL MEAN OF SITES IN YOUNGER INTRUSIVE ROCKS (37, 38 = CAPE CROSS COMPLEX ; 44, 45 = ERONGO GRANITE ; 43 = BRANDBERG GRANITE)

E ⊡ OVERALL MEAN OF SITES APPROXIMATING TO GEOMAGNETIC POLE DIRECTION

⌖ GEOMAGNETIC POLE DIRECTION (PRESENT)

F ■ MEAN OF UNMETAMORPHOSED NOSIB ROCKS (F' = ANTIPOLE) (AFTER MC ELHINNY AND MC WILLIAMS, 1977 ; HENTHORN, 1978)

* FISHER STATISTICS AS DEFINED IN TEXT

Fig 12 Wulff projection of site-mean magnetisation directions of Damara Sequence and basement rocks, and of late-, to post-Karoo intrusives (north seeking vector on upper hemisphere, open symbols; on lower hemisphere, closed symbols. The primitive plane is the present horizontal at the sampling sites).

Those sites which yielded statistically significant within-site means, at the 95% level of confidence (listed in Table II), are plotted stereographically in Fig 12. Five distinct between-site groupings of remanent direction are evident (Table V). No structural corrections were applied to the site-mean directions in view of the relatively close grouping of the data points, particularly of Group A, which were derived from localities of highly variable structural orientation. The initial assumption (Section 4.0) that the remanent magnetisation at the time of deposition of the Damara rocks had been completely overprinted by the 500 Ma orogenic event, and that no subsequent movement had taken place, appears to be valid. The magnetisation resulting in the Group A direction is thus postdeformational.

TABLE V : MEAN DIRECTIONS OF MAGNETISATION AND PALAEOMAGNETIC POLE POSITIONS

GROUP*	MEAN DIRECTION		FISHER STATISTICS				VIRTUAL GEOMAGNETIC POLE	
	DECLINATION°	INCLINATION°	k	$\alpha 95°$	R	n	LATITUDE°	LONGITUDE°
A	334,4	54,5	35	5,0	23,34	24	27,5	351,4
B	158,1	-21,3	22	56,2	1,95	2	-50,5	159,2
C	143,2	-43,0	17	22,6	3,83	4	-29,8	156,2
D	322,6	-43,7	14	21,4	4,71	5	56,0	273,0
E	359,8	-52,2	42	14,3	3,93	4	Close to present day	

* As defined in Fig 12

The significance of these groupings is discussed separately below according to the formational units in which they occur.

<u>Basement rocks</u>

Of the three sites sampled within the core of the orogenic belt in rocks of the Abbabis Metamorphic Complex (Sites 35 and 36) and adjacent granite gneiss (site 34) only sites 34 and 35 were stable after cleaning at 50 mT. These two sites displayed significant groupings which yielded directions similar to those of the Nosib rocks of Group A indicating that they had either become entirely remagnetised with the Group A direction or that this secondary magnetisation had affected domains of high coercivity which could not be demagnetised in the available alternating fields.